Interface enhanced well-dispersed Co_9S_8 nanocrystals as an efficient polysulfide host in lithium–sulfur batteries

Xue Liu [a,c,1], Qiu He [b,1], Hong Yuan [c], Chong Yan [d], Yan Zhao [b], Xu Xu [a], Jia-Qi Huang [d], Yu-Lun Chueh [e], Qiang Zhang [c,*], Liqiang Mai [a,*]

[a] State Key Laboratory of Advanced Technology for Materials Synthesis and Processing, Wuhan University of Technology, Wuhan 430070, Hubei, China
[b] State Key Laboratory of Silicate Materials for Architectures, Wuhan University of Technology, Wuhan 430070, Hubei, China
[c] Beijing Key Laboratory of Green Chemical Reaction Engineering and Technology, Department of Chemical Engineering, Tsinghua University, Beijing 100084, China
[d] Advanced Research Institute of Multidisciplinary Science, Beijing Institute of Technology, Beijing 100081, China
[e] Department of Materials Science and Engineering, Taiwan Tsinghua University, Hsinchu 30013, Taiwan, China

ARTICLE INFO

ABSTRACT

The high specific capacity and energy density of lithium–sulfur batteries have attracted strong considerations on their fundamental mechanism and energy applications. However, polysulfide shuttle is still the key issue that impedes the development of Li–S batteries. Exploring nanocrystal hosts for polysulfide immobilization and conversion is a promising way. In this contribution, we have investigated well-dispersed Co_9S_8 nanocrystals grown on graphene oxide (GO) nanosheets with different degrees of dispersion as cathode host materials for Li–S batteries. The Co_9S_8-GO composite with 1 wt% GO (GCS1) has an average crystal size of 76 nm and shows the strongest adsorption capability toward lithium polysulfides. When used as the host material for the cathode of Li–S batteries, the GCS1-sulfur composite exhibits an initial specific capacity of ~1000 mAh g^{-1} at 0.5 C and shows an average decay rate of 0.11% for 500 cycles. This work on the dispersion control of Co_9S_8 nanocrystals may inspire more investigations on well-dispersed nanocrystal based hosts for Li–S batteries.

1. Introduction

Lithium-ion batteries (LIBs) have been a mature energy storage technique for electrochemical energy storage after more than 30 years' research and development (R&D). However, its relatively low specific capacity and energy density have caused range anxiety in electric vehicles [1,2]. Lithium-sulfur (Li–S) batteries, which have a theoretical specific capacity of 1675 mAh g^{-1}, are considered to be one of the most promising energy storage systems for high energy-consumption equipments [3–6]. For example, through the utilization of lithium-sulfur batteries as the power source, the goal of 500-mile range of electric cars in a single charge is highly expected. However, there are many bottlenecks blocking the practical use of Li–S batteries [7–13]. On the cathode part, there exist three main classic problems. The first issue is the polysulfide

shuttling process, during which soluble polysulfides shuttle to the lithium anode and react with it and then shuttle back to the cathode. The second aspect is the low conductivity of sulfur and its solid product after lithiation. The third one is the volume changes of sulfur during lithiation and delithiation.

Many solutions have been put forward to investigate the fundamental mechanism and electrochemical performance optimization approaches of Li–S batteries. Various sulfur host materials have been proposed, mainly in two categories, non-polar and polar ones. The former is generally the diversified nanostructured carbon materials, such as mesoporous carbon [14,15], graphene [16,17], carbon nanotubes [18,19] and so on, which have weak binding energies with lithium polysulfides. The latter are mainly doped carbon materials [20,21], conductive oxygen-deficient titanium oxides [22–25], metallic cobalt sulfides [26–29], catalytic MnO_2 [30–32], bifunctional perovskites [33], metal nitrides [34–36], heterostructures [37–39] and so on [40,41]. Based on the previous researches, many properties of the host materials influencing the performance of Li–S batteries are summarized [42], such as the adsorption
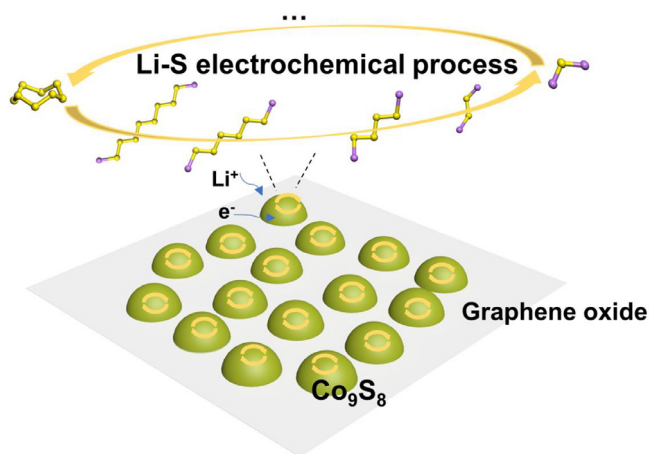

Fig. 1. Illustration of the Co_9S_8-GO composite in contributing to the Li–S electrochemical cycling. Dispersed on graphene oxide nanosheet, Co_9S_8 nanocrystals can efficiently catalyze the redox reaction in Li–S batteries.

capability of polysulfides, electronic conductivity, surface area, porosity volume and distribution, catalytic conversion of lithium polysulfides/sulfides, etc. However, little attention has been paid to the influence of dispersion of supported nanocrystals on the electrochemical performances of Li–S batteries. Recently, the "polysulfide catalysis" concept is gaining more and more interest in Li–S batteries. In fact, polysulfide conversion is a process where nanocatalysts are needed as mediators [9,43]. Dispersion is a concept of much importance in heterogeneous catalysis because only exposed surface atoms can contribute to the catalytic reactions [44]. In heterogeneous catalysis, dispersion often comes together with particle sizes and increases with the decrease of particle sizes. Previous studies showed that metal catalysts such as Pt-graphene can effectively reduce the overpotential of the polysulfide reduction [45]. So it is of much significance to investigate nanocrystal based host materials with a proper degree of dispersion in Li–S batteries.

Nanostructured conductive metal sulfide (such as Co_9S_8) catalysts can effectively adsorb polysulfides and accelerate the conver-

sion between soluble lithium polysulfides and solid lithium sulfides [27,28,46,47]. Herein, we investigated well-dispersed Co_9S_8 nanocrystals grown on graphene oxide nanosheets with different degrees of dispersion as cathode host materials for Li–S batteries. With graphene oxides (GO) incorporated in the composites increasing its contents, Co_9S_8 nanocrystals exhibited higher dispersity and smaller sizes. Fig. 1 illustrates the composite and its efficient function in regulating polysulfide adsorption and conversion in Li–S batteries. Compared to bulk Co_9S_8 with the same weight, the Co_9S_8-GO composite has more individual Co_9S_8 nanocrystals and shows more active sites toward lithium polysulfides. However, when used as polysulfide host materials in Li–S batteries, well-dispersed Co_9S_8 nanocrystals with a proper content of graphene oxides delivered the best electrochemical performances. The Co_9S_8-GO composite with 1 wt% GO (GCS1) and an average crystal size of 76 nm showed the best cycling stability in Li–S batteries among the series.

2. Results and discussion

The powder X-ray diffraction (XRD) patterns (Fig. 2(a)) of the as-prepared Co_9S_8 and Co_9S_8-GO composites with different amounts of GO confirm that Co_9S_8 exists in the composites with the cobalt pentlandite crystallographic phase which can be indexed to cubic Co_9S_8 (JCPDS Card No. 03-065-1765, space group *Fm-3m*). The two most intensive peaks at 29.8° and 52.1° correspond to the diffractions of (311) and (440) planes respectively. No obvious peak can be observed in the patterns around the 26° because the low content of graphene and relatively low diffraction intensity of graphene. Based on the weight ratios of GO to $Co(NO_3)_2 \cdot 6H_2O$ when synthesizing the composites, they were named GCS0 (0 wt% GO), GCS1 (1 wt% GO) and GCS4 (4.1 wt% GO). In order to compare the nanocrystal sizes of GCS1 and GCS4, we used Scherrer formula to calculate the average crystallite size by selecting the (311) facet diffraction peak as a representative. As shown in Table S1, on average, the crystallite size of GCS1 and GCS4 are 38 and 33 nm, respectively. This indicates that graphene oxide can promote the nucleation of Co_9S_8 nanocrystals and reduce its average sizes.

The surface area and pore distribution of these materials were measured by N_2 adsorption/desorption isotherm analysis. The
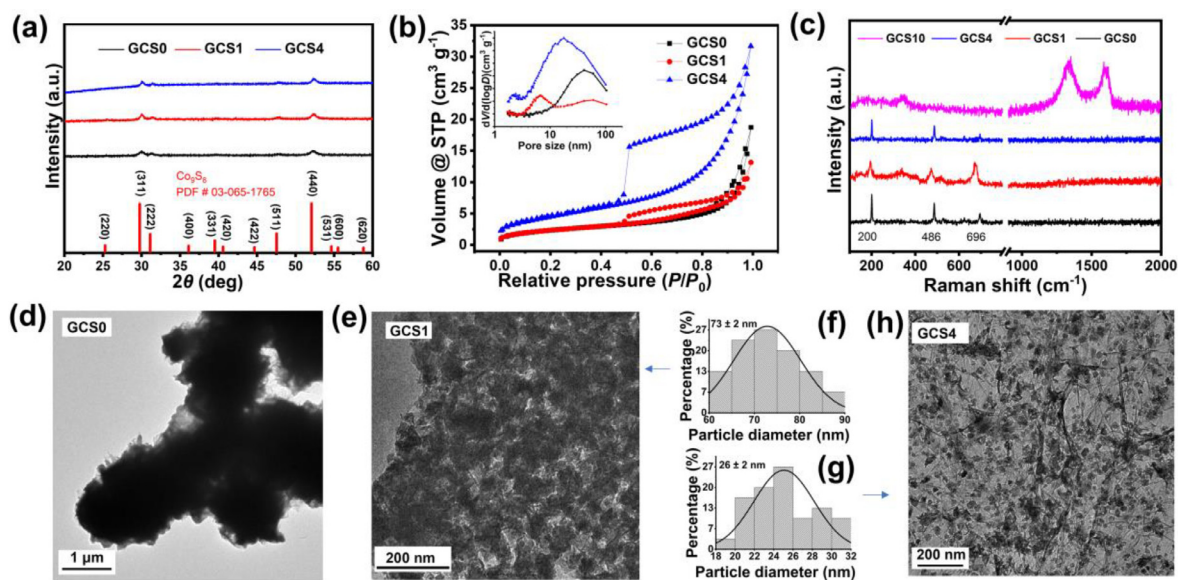

Fig. 2. (a) PXRD patterns of GCS0, GCS1 and GCS4 and the indexed PDF card. (b) N_2 adsorption/desorption isotherms of GCS0, GCS1 and GCS4, inset is the pore distribution curve of them. (c) Raman spectra of GCS0, GCS1, GCS4 and GCS10. TEM images of (d) GCS0, (e) GCS1 and (h) GCS4 and corresponding size distribution diagrams of (f) GCS1 and (g) GCS4.

curves for GCS0, GCS1 and GCS4 and the corresponding pore distribution curves (inset) are shown in Fig. 2(b). GCS1 and GCS4 have a type IV physisorption isotherm, while it is type II for GCS0. It means that both GCS1 and GCS4 have mesopores while GCS0 has macropores. The hysteresis loops of GCS0, GCS1 and GCS4 are H3 type, which indicates that there exist slit type pores in these materials. The surface area of GCS0, GCS1 and GCS4 are 8.5, 8.5 and 16.5 m^2 g^{-1}, respectively (Table S1). Elemental analysis was conducted to examine the carbon and nitrogen content of GCS1 and GCS4 and the data are shown in Table S2. The carbon and nitrogen content of GCS1 is 2.8 wt% and 1.32 wt% with a C/N ratio of 2.1. For GCS4, the carbon content is 7.9 wt%, nitrogen content is 1.4 wt% and the C/N ratio is 5.6. The nitrogen should be from the solvent dimethylformamide which doped graphene with nitrogen atoms. The Raman spectra of GCS0, GCS1 and GCS4 are shown in Fig. 2(c). In the range of 100–1000 cm^{-1}, the most intensive peaks are located at around 200, 486 and 696 cm^{-1}, which should be ascribed to the existence of Co_9S_8 [48,49]. In the range of 1000–2000 cm^{-1}, no D or G peaks related to the existence of graphene is observed. However, GCS10 exhibited a very different Raman spectrum compared to them. No intense characteristic signals of Co_9S_8 are found in GCS10 while D and G peaks are obvious (Fig. 2(c), purple). This indicates that the content of graphene is so high that GCS10 is more like a carbon material rather than Co_9S_8-dominating material.

The transmission electron microscopy (TEM) images confirm that ultrafine nanocrystals of Co_9S_8 are well dispersed on graphene nanosheets. Fig. 2(d) reveals that GCS0 is made up of bulk Co_9S_8 solids. The size of every single Co_9S_8 particle is about one micrometer. Fig. 2(e) and (h) exhibits the morphology of GCS1 and GCS4, respectively. The Co_9S_8 nanocrystals with different sizes disperse and anchor on the wrinkled graphene nanosheets in GCS1 and GCS4. Fig. 2(f) and (g) is the corresponding nanocrystal size distribution diagrams. The size of nanocrystals of GCS1 is about 73 nm while it decreases to 26 nm in GCS4. The content of GO plays a vital role in the morphology of resulting samples. GO here has mainly two functions in the synthesis procedure. Firstly, GO can provide a platform for Co_9S_8 nanocrystals to nucleate and grow on the carbon nanosheet with oxygen-containing functional groups and defects. Secondly, the oxygen-containing functional groups on the carbon nanosheets of GO make it a good anionic surfactant, which can avoid the aggregation of Co_9S_8 nanocrystals. Without the existence of graphene oxide, Co_9S_8 grows freely in the dimethyl formamide (DMF) solvent and results in a nanosheets-constructed flower-like nanostructure (Fig. S1(a)).

Conductivity is crucial to the electron transfer process during the electrochemical process in Li–S batteries. Symmetrical cells comprised of GCSx (x = 0 or 1 or 4, the same below) electrodes and the Li_2S_8 electrolyte was constructed. Through electrochemical impedance spectroscopy (EIS) analysis, the cell with the GCS0 electrode showed the lowest impedance of about 4 kΩ. For cells with GCS1 and GCS4, it was around 5 kΩ, but the former was a little smaller than the latter (Fig. 3(a)). This result showed that the addition of graphene oxide decreased the overall electron conductivity of the composite materials. Moreover, the catalytic capability toward polysulfides reduction is also a vital parameter that decides the specific capacity of Li–S batteries. Cyclic voltammetry (CV) was used to differentiate the capability of GCS0, GCS1 and GCS4 in catalyzing polysulfides reduction. As shown in Fig. 3(b), symmetrical cells with GCS0, GCS1 and GCS4 show similar hysteresis loop-like curves. However, at the highest overpotential, GCS1 shows the highest current density and GCS4 exhibits the lowest. It indicates that GCS1 has the largest capability in catalyzing the conversion of polysulfides, which is also confirmed by the long-cycle performance of Li–S batteries afterwards. Polysulfide adsorption capability is also a very important parameter that determines the perfor-

mance of a host material employed as the cathode material in Li–S batteries. The visualization experiment was conducted to compare the capability of polysulfides adsorption of GCS0, GCS1 and GCS4. Fig. 3(e) shows that the Li_2S_8 in DOL/DME solvent is a dark red solution. With the addition of GCS0, GCS1 and GCS4 (the same weight) into Li_2S_8 solutions in different test tubes, after a rest for 24 h, the color of the supernatant became distinctly different. GCS1 interacted with polysulfides strongly and the supernatant of the test tube with it became very clear. However, GCS0 showed weak adsorption capability toward polysulfides and the color of the supernatant of the test tube with it still kept dark red, a little lighter than the original Li_2S_8 solution. GCS4's adsorption capability was in between GCS1 and GCS0 and the color of its supernatant was light dark red. This experiment shows that GCS1 is the strongest in polysulfides adsorption, GCS4 is the second and GCS0 is the weakest.

X-ray photon spectroscopy (XPS) was used to detect the interactions between GCSx and lithium polysulfides (here is Li_2S_8). The mixtures were collected from the precipitates by centrifuging the GCSx-Li_2S_8 liquids. As shown in Fig. 3(c), the Co 2p spectrum exhibits two contributions from Co $2p_{3/2}$ and Co $2p_{1/2}$. For GCS0, the peaks at 780.88 and 797.28 eV should be assigned to the state of Co^{3+} and the peaks at 782.68 and 803.38 eV should be assigned to the state of Co^{2+}[50]. In the case of the GCS0-Li_2S_8 mixture, peaks at 777.68 and 792.86 eV are due to the existence of Co^{3+} and peaks at 779.68 and 795.98 eV should be assigned to the state of Co^{2+}. The XPS spectra of GCS1-Li_2S_8 and GCS4-Li_2S_8 mixture are very similar and show characteristic peaks at nearly the same locations. For example, in the case of GCS1-Li_2S_8 mixture, characteristic peaks of the state of Co^{3+} are located at 777.78 and 792.78 eV and Co^{2+} are at 779.78 and 795.78 eV. The peaks of Co $2p_{3/2}$ in GCS0 decreased about 3.1 eV compared to that in the mixture of GCS1-Li_2S_8. However, there is ca. 0.1 eV change of the peaks between the GCS0-Li_2S_8 and GCS1-Li_2S_8 mixture. This result shows that the interactions between GCSx and polysulfides are very strong (up to 3.0 eV variation), which should be ascribed to the polar property of Co_9S_8. The similarities between the three GCSx-Li_2S_8 (x = 0, 1, 4) mixtures indicate that XPS is hard to differentiate the polysulfides adsorption capabilities of GCSx. Fig. 3(d) depicts the S 2p spectrums of GCS0 and GCSx-Li_2S_8 mixtures. Following convention, only S $2p_{3/2}$ will be mentioned in the $S_{2p3/2}/S_{2p1/2}$ doublet. The spectrum of Li_2S_8 exhibit two $2p_{3/2}$ contributions at 162.88 and 163.48 eV, respectively. The former peak should be assigned to the state of bridging sulfur (S-S). The latter should be assigned to the terminal sulfur. There is a broad peak at above 165 eV and it can be ascribed to the partial oxidation of Li_2S_8 during transfer when testing. In the sample of the GCS0-Li_2S_8 mixture, two $2p_{3/2}$ contributions are located at 160.38 and 161.78 eV, representing a −2.5 and −1.7 eV shift, respectively. GCS1-Li_2S_8 and GCS4-Li_2S_8 mixtures show similar spectrums with the GCS0-Li_2S_8 mixture. No more than 0.2 eV shift exists in the peaks. This result indicates that the existence of Co_9S_8 changed the chemical environment of sulfur greatly. Also, like the Co 2p spectrum, the interactions of GCSx and polysulfides are hard to be distinguished from the S 2p spectrum. The Li 1s spectrums show that there is ca. 1 eV shift from Li_2S_8 to the GCSx-Li_2S_8 sample (Fig. S2). It corroborates the strong interactions between GCSx and polysulfides. In order to uncover the strong interactions between Co_9S_8 and lithium polysulfides, we employed density functional theory (DFT) calculations to investigate the intrinsic origins. The Co_9S_8 (440) lattice plane with atomic composition ratio of Co:S = 1:1 on exposed surfaces is taken as the representative because it exhibits the strongest diffraction peak in the XRD pattern. Fig. 4(a) depicts the optimized structure of Co_9S_8(440). The adsorption energies of Li_2S_4, Li_2S_8 on the Co_9S_8(440) plane are −3.67, −4.04 eV (Fig. 4(b) and (c)), respectively.
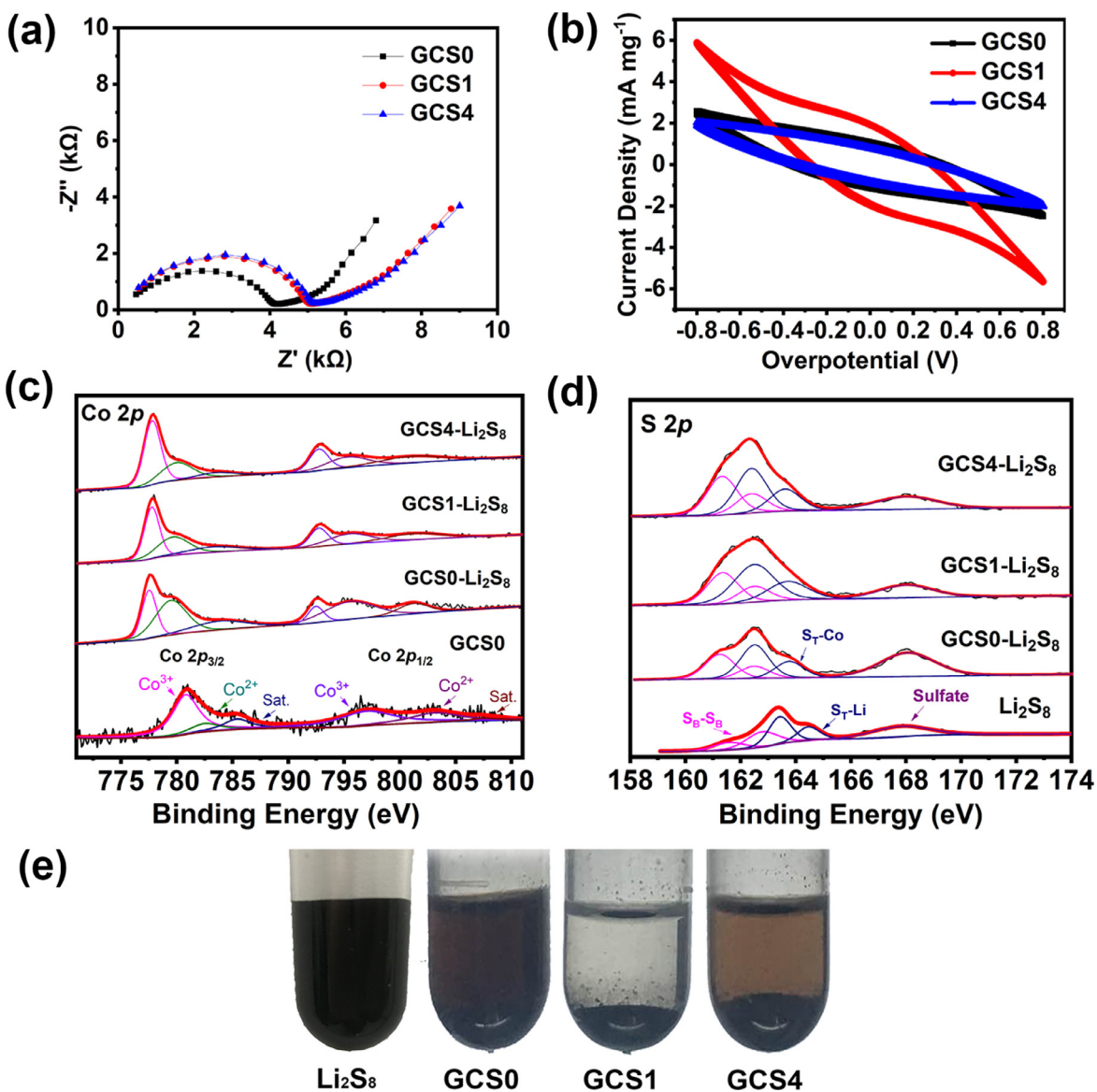
Fig. 3. (a) EIS curves (b) CV curves of symmetrical cells with GCS0, GCS1 and GCS4 as electrodes and Li_2S_8 as the electrolyte. XPS spectrums of (c) Co 2p in GCS0, GCS0-Li_2S_8, GCS1-Li_2S_8 and GCS4-Li_2S_8 mixtures and (d) S 2p in Li_2S_8, GCS0-Li_2S_8, GCS1-Li_2S_8 and GCS4-Li_2S_8 mixtures. (e) Digital photographs of Li_2S_8, and its mixtures with GCS0, GCS1 and GCS4 (from left to right) in the DOL/DME solvent.
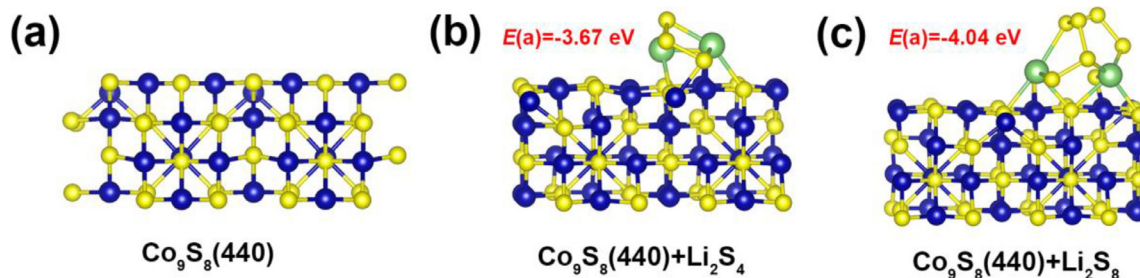

Fig. 4. (a) The optimized structures of the Co_9S_8(440) surface and its adsorption models of binding with (b) Li_2S_4 and (c) Li_2S_8, respectively.

Batteries with solid sulfur cathodes were tested through CV and electrochemical cycling to compare the effects of GCS0, GCS1 and GCS4 on the electrochemical performances of Li–S batteries. The active sulfur cathode material was made by melt-diffusing sulfur in the GCSx material at 155 °C. The powder XRD patterns are shown in Fig. S3. Characteristic peaks originated from sulfur are obvi-

ous while peaks from Co_9S_8 have disappeared. Thermogravimetric analysis was used to test the sulfur content in GCSx-S composites. As shown in Fig. S4, the sulfur content in GCS0-S, GCS1-S and GCS4-S composites are 71 wt%, 72 wt% and 72 wt%, respectively. The CV curves of GCS0, GCS1 and GCS4 were obtained through scanned at 0.1 mV s^{-1} in the potential window of 1.7–2.8 V
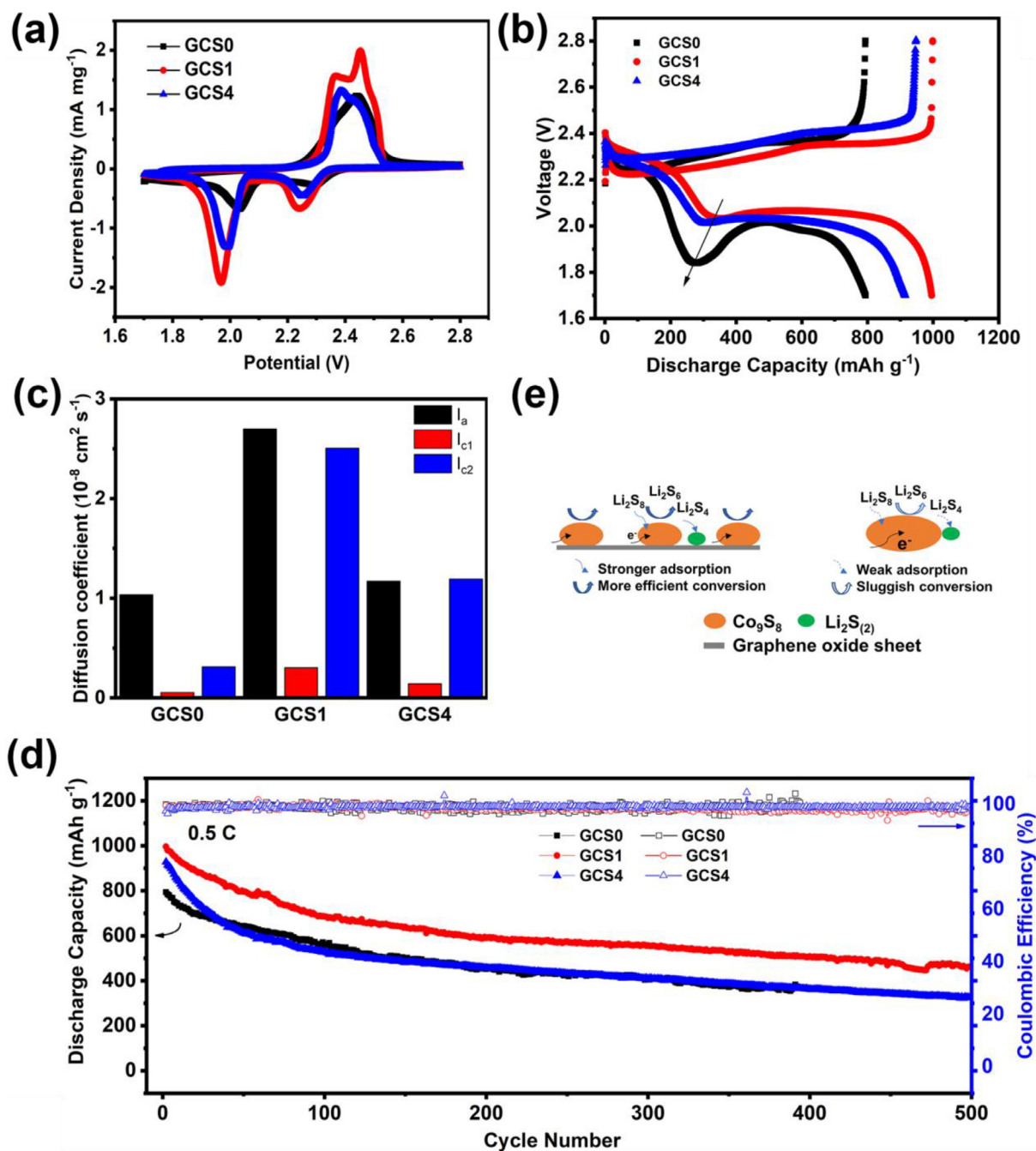
Fig. 5. (a) CV curves scanned at 0.1 mV s^{-1}, (b) Typical charge/discharge voltage curves at 0.5 C, (c) Calculated lithium ion diffusion coefficients from three redox peaks of the corresponding CV curves (I_a, I_{c1} and I_{c2} correspond to the anodic peak, first cathodic peak and second cathodic peak, respectively) and (d) Long-term cycling curves at 0.5 C of the Li–S batteries enabled by GCS0-S, GCS1-S and GCS4-S composites. (e) Comparison of different electrochemical mechanisms of GCS1 (left) and GCS0 (right) in Li–S batteries.

(Fig. 5(a)). There are two cathodic peaks and one anodic peak for every kind of material. Following the method widely used in electrocatalysis, the onset potential for every peak was taken at a current density of 10 μA cm^{-2} beyond the baseline current where the change of current is the smallest, i.e. dI/dV=0. For GCS1, the onset potential for the first cathodic peak is 2.366 V which is 27 mV lower than GCS0 but 2 mV higher than GCS4. It is 2.070 V for the second onset potential of GCS1, 28 mV lower than GCS0 and 137 mV higher than GCS4. For the anodic peaks, they are 2.157, 2.189 and 2.191 V for GCS0, GCS1 and GCS4, respectively. It indicates that GCS0 has the largest onset potential for the cathodic process and the lowest onset potential for the anodic process. It

should be ascribed the highest electronic conductivity of GCS0. Moreover, the peak voltages were also investigated. They are 2.293, 2.251 and 2.241 V for the first cathodic peak of GCS0, GCS1 and GCS4, respectively. For the second cathodic peak, they are 2.030, 1.991 and 1.969 V for GCS0, GCS1 and GCS4, respectively. Because the anodic peak is a combined peak of several oxidation reactions of polysulfides, so it has no sense to compare the anodic peak voltages of different materials. Through analyzing the trend of change of cathodic peak voltages, we found that it had a similar tendency to the onset potential, which should also be ascribed to the intrinsic conductivity of GCS0, GCS1 and GCS4. Besides, the rate of lithium ion diffusion within the electrodes in Li–S batteries has

an essential effect on the conversion process of sulfur redox. We took advantage of the classical Randles−Sevcik equation to calculate the lithium diffusion coefficient (D_{Li+}) based on cathodic current peaks I_{c1} and I_{c2} and the highest anodic current peak I_a (Fig. 5(c) and Table S3) [51–53]. For the reduction process, D_{Li+} coefficients of GCS1 and GCS4 are an order of magnitude higher than that of GCS0. GCS1 is a little higher than GCS4. However, for the oxidation process, D_{Li+} coefficients of GCS0, GCS1 and GCS4 are at the same order of magnitude. GCS1 still has the highest D_{Li+} coefficient. This indicates that GCS1 and GCS4 showed a higher activity in catalyzing the reduction process of sulfur species compared to the oxidation process.

Typical galvanostatic discharge/charge voltage curves of GCS0, GCS1 and GCS4 at 0.5 C were also investigated in the potential range of 1.7–2.8 V. Fig. 5(b) shows that there are usually two plateaus in the discharge process and one plateau in the charge process for every specific material. GCS0 showed a very sluggish kinetic discharge process. For example, there is a deep ditch (black arrow) at the nexus of liquid-liquid single-phase reduction and liquid-solid two-phase reduction, which was analyzed by a former review [54]. If the host material could not adsorb the polysulfides efficiently, the kinetic rate became very low and the potential drop would become obvious too. It corroborates the low efficiency of GCS0 in adsorbing polysulfides because at this point polysulfides solution has the largest viscosity. It is in highly accordance with the former visualization test. As expected, GCS1 has the highest kinetic rate in the discharge process. What is more, the voltage hysteresis between the discharge and charge process for GCS1 is about 250 mV and is the lowest amongst the three materials. For practical use of Li–S batteries, we conducted a long-term cycling test of the Li–S batteries enabled by GCS0, GCS1 and GCS4 (Fig. 5(d)). After activation for several cycles, GCS1 showed an initial specific capacity of ~1000 mAh g^{-1} and kept a retention of ~59% after 200 cycles and of ~46% after 500 cycles. However, GCS0 showed its initial specific capacity of ~800 mAh g^{-1} and a retention of ~57% after 200 cycles. For GCS4, its first specific capacity was about 930 mAh g^{-1} and it retained ~50% after 200 cycles. The capacity fading rate for GCS0, GCS1 and GCS4 in the 300 cycles are 0.16%, 0.14% and 0.18%, respectively. For GCS1, its capacity fading rate in the 500 cycles is 0.11%.

Based on the above results, we can conclude that GCS1 has the strongest capability of adsorption toward polysulfides. GCS1 has more active sites (Co_9S_8 nanocrystals) than bulk Co_9S_8, which guarantees higher adsorption toward soluble lithium polysulfides (Li_2S_n, $4 \leq n \leq 8$) and more efficient conversion of them to solid Li_2S_2 and Li_2S (Fig. 5(e)). Even though GCS4 possess smaller Co_9S_8 nanocrystals, the interfaces of Co_9S_8 and graphene oxide should be less than GCS1 because it has a higher content of bare GO, which is not the best ratio in the composite. That is why GCS1 can adsorb more lithium polysulfides than GCS4. Moreover, although its conductivity is not the highest, it still exhibits the best electrochemical performance when employed as the cathode host material in Li–S batteries. Higher conductivity will contribute to higher onset potentials in the cathodic process and lower onset potentials in the anodic potentials. All in all, polysulfide adsorption is the most important parameter that determines the rate of discharge/charge reactions, specific capacity and cycling stability of Li–S batteries.

3. Conclusions

In summary, we have investigated the influence of well-dispersed metal sulfides (Co_9S_8) grown on graphene nanosheets with different degrees of dispersion (GCS1 and GCS4) as host materials on the electrochemical performances of Li–S batteries. The visual polysulfide adsorption test showed that GCS1 had the strongest capability toward the adsorption of lithium polysulfides.

The electronic conductivity, lithium ion diffusion rate and catalytic contribution of polysulfide conversion of GCS0, GCS1 and GCS4 have been compared too. GCS1 exhibits the best electrochemical performance when employed as the cathode host material in Li–S batteries. It should be ascribed to its largest capability in polysulfides adsorption and good catalytic contribution of polysulfides conversion. What is more, GCS1 facilitates the lithium ion diffusion most among the three materials. This work may inspire more research on supported nanocrystal catalysts with different degrees of dispersion for polysulfides conversion and its contribution in improving practical uses of Li–S batteries.

Declaration of Competing Interest

The authors declare that they have no known competing financial interests or personal relationships that could have appeared to influence the work reported in this paper.

Acknowledgments

Supplementary materials

Supplementary material associated with this article can be found, in the online version, at doi:10.1016/j.jechem.2020.01.003.

References

[1] J.W. Choi, D. Aurbach, Nat. Rev. Mater. 1 (2016) 16013.
[2] M. Li, J. Lu, Z. Chen, K. Amine, Adv. Mater. 30 (2018) 1800561.
[3] A. Manthiram, Y. Fu, S.-H. Chung, C. Zu, Y.-S. Su, Chem. Rev. 114 (2014) 11751–11787.
[4] Q. Pang, X. Liang, C.Y. Kwok, L.F. Nazar, Nat. Energy 1 (2016) 16132.
[5] R. Fang, S. Zhao, Z. Sun, D.-W. Wang, H.-M. Cheng, F. Li, Adv. Mater. 29 (2017) 1606823.
[6] Y. Liang, C.-Z. Zhao, H. Yuan, Y. Chen, W. Zhang, J.-Q. Huang, D. Yu, Y. Liu, M.-M. Titirici, Y.-L. Chueh, InfoMat 1 (2019) 6–32.
[7] Z.W. Seh, Y. Sun, Q. Zhang, Y. Cui, Chem. Soc. Rev. 45 (2016) 5605–5634.
[8] H.-J. Peng, J.-Q. Huang, X.-B. Cheng, Q. Zhang, Adv. Energy Mater. 7 (2017) 1700260.
[9] D. Liu, C. Zhang, G. Zhou, W. Lv, G. Ling, L. Zhi, Q.-H. Yang, Adv. Sci. 5 (2018) 1700270.
[10] S.-Y. Li, W.-P. Wang, H. Duan, Y.-G. Guo, J. Energy Chem. 27 (2018) 1555–1565.
[11] L. Kong, Q. Jin, X.-T. Zhang, B.-Q. Li, J.-X. Chen, W.-C. Zhu, J.-Q. Huang, Q. Zhang, J. Energy Chem. 39 (2019) 17–22.
[12] B. Liu, R. Fang, D. Xie, W. Zhang, H. Huang, Y. Xia, X. Wang, X. Xia, J. Tu, Energy Environ. Mater. 1 (2018) 196–208.
[13] W. Guo, Y. Fu, Energy Environ. Mater. 1 (2018) 20–27.
[14] X. Ji, K.T. Lee, L.F. Nazar, Nat. Mater. 8 (2009) 500–506.
[15] J. Schuster, G. He, B. Mandlmeier, T. Yim, K.T. Lee, T. Bein, L.F. Nazar, Angew. Chem. Int. Ed. 51 (2012) 3591–3595.
[16] M.-Q. Zhao, Q. Zhang, J.-Q. Huang, G.-L. Tian, J.-Q. Nie, H.-J. Peng, F. Wei, Nat. Commun. 5 (2014) 3410.
[17] R. Fang, S. Zhao, S. Pei, X. Qian, P.-X. Hou, H.-M. Cheng, C. Liu, F. Li, ACS Nano 10 (2016) 8676–8682.
[18] M.-Q. Zhao, H.-J. Peng, G.-L. Tian, Q. Zhang, J.-Q. Huang, X.-B. Cheng, C. Tang, F. Wei, Adv. Mater. 26 (2014) 7051–7058.
[19] H.-J. Peng, J.-Q. Huang, M.-Q. Zhao, Q. Zhang, X.-B. Cheng, X.-Y. Liu, W.-Z. Qian, F. Wei, Adv. Funct. Mater. 24 (2014) 2772–2781.
[20] C. Tang, Q. Zhang, M.-Q. Zhao, J.-Q. Huang, X.-B. Cheng, G.-L. Tian, H.-J. Peng, F. Wei, Adv. Mater. 26 (2014) 6100–6105.
[21] H.-J. Peng, T.-Z. Hou, Q. Zhang, J.-Q. Huang, X.-B. Cheng, M.-Q. Guo, Z. Yuan, L.-Y. He, F. Wei, Adv. Mater. Interfaces 1 (2014) 1400227.
[22] Q. Pang, D. Kundu, M. Cuisinier, L.F. Nazar, Nat. Commun. 5 (2014) 4759.
[23] X. Tao, J. Wang, Z. Ying, Q. Cai, G. Zheng, Y. Gan, H. Huang, Y. Xia, C. Liang, W. Zhang, Nano Lett 14 (2014) 5288–5294.
[24] S. Mei, C.J. Jafta, I. Lauermann, Q. Ran, M. Kärgell, M. Ballauff, Y. Lu, Adv. Funct. Mater. 27 (2017) 1701176.

[25] Y. Wang, R. Zhang, J. Chen, H. Wu, S. Lu, K. Wang, H. Li, C.J. Harris, K. Xi, R.V. Kumar, Adv. Energy Mater. (2019) 1900953.

[26] Z. Yuan, H.-J. Peng, T.-Z. Hou, J.-Q. Huang, C.-M. Chen, D.-W. Wang, X.-B. Cheng, F. Wei, Q. Zhang, Nano Lett 16 (2016) 519–527.

[27] Q. Pang, D. Kundu, L.F. Nazar, Mater. Horiz. 3 (2016) 130–136.

[28] H. Lin, S. Zhang, T. Zhang, S. Cao, H. Ye, Q. Yao, G.W. Zheng, J.Y. Lee, ACS Nano 13 (2019) 7073–7082.

[29] X. Chen, H.-J. Peng, R. Zhang, T.-Z. Hou, J.-Q. Huang, B. Li, Q. Zhang, ACS Energy Lett. 2 (2017) 795–801.

[30] X. Liang, C. Hart, Q. Pang, A. Garsuch, T. Weiss, L.F. Nazar, Nat. Commun. 6 (2015) 5682.

[31] Z. Li, J. Zhang, X.W.D. Lou, Angew. Chem. Int. Ed. 54 (2015) 12886–12890.

[32] C. Lin, L. Qu, J. Li, Z. Cai, H. Liu, P. He, X. Xu, L. Mai, Nano Res 12 (2019) 205–210.

[33] L. Kong, X. Chen, B.-Q. Li, H.-J. Peng, J.-Q. Huang, J. Xie, Q. Zhang, Adv. Mater. 30 (2018) 1705219.

[34] Z. Cui, C. Zu, W. Zhou, A. Manthiram, J.B. Goodenough, Adv. Mater. 28 (2016) 6926–6931.

[35] Z. Sun, J. Zhang, L. Yin, G. Hu, R. Fang, H.-M. Cheng, F. Li, Nat. Commun. 8 (2017) 14627.

[36] Z. Li, Q. He, X. Xu, Y. Zhao, X. Liu, C. Zhou, D. Ai, L. Xia, L. Mai, Adv. Mater. 30 (2018) 1804089.

[37] T. Zhou, W. Lv, J. Li, G. Zhou, Y. Zhao, S. Fan, B. Liu, B. Li, F. Kang, Q.-H. Yang, Energy Environ. Sci. 10 (2017) 1694–1703.

[38] C. Ye, Y. Jiao, H. Jin, A.D. Slattery, K. Davey, H. Wang, S.-Z. Qiao, Angew. Chem. Int. Ed. 57 (2018) 16703–16707.

[39] L. Jiao, C. Zhang, C. Geng, S. Wu, H. Li, W. Lv, Y. Tao, Z. Chen, G. Zhou, J. Li, Adv. Energy Mater. (2019) 1900219.

[40] B.-Q. Li, H.-J. Peng, X. Chen, S.-Y. Zhang, J. Xie, C.-X. Zhao, Q. Zhang, CCS Chem 1 (2019) 128–137.

[41] D. An, L. Shen, D. Lei, L. Wang, H. Ye, B. Li, F. Kang, Y.-B. He, J. Energy Chem. 31 (2019) 19–26.

[42] X. Liu, J.-Q. Huang, Q. Zhang, L. Mai, Adv. Mater. 29 (2017) 1601759.

[43] W.-G. Lim, S. Kim, C. Jo, J. Lee, Angew. Chem. Int. Ed. 58 (2019) 18746–18757.

[44] O. Deutschmann, H. Knözinger, K. Kochloefl, T. Turek, Ullmann's Encyclopedia of Industrial Chemistry, American Cancer Society, 2009.

[45] H. Al Salem, G. Babu, C.V. Rao, L.M.R. Arava, J. Am. Chem. Soc. 137 (2015) 11542–11545.

[46] T. Chen, L. Ma, B. Cheng, R. Chen, Y. Hu, G. Zhu, Y. Wang, J. Liang, Z. Tie, J. Liu, Nano Energy 38 (2017) 239–248.

[47] J. He, Y. Chen, A. Manthiram, Energy Environ. Sci. 11 (2018) 2560–2568.

[48] Y. Wang, Y. Wang, Y. Wang, X. Feng, W. Chen, J. Qian, X. Ai, H. Yang, Y. Cao, ACS Appl. Mater. Interfaces 11 (2019) 19218–19226.

[49] L.-L. Feng, G.-D. Li, Y. Liu, Y. Wu, H. Chen, Y. Wang, Y.-C. Zou, D. Wang, X. Zou, ACS Appl. Mater. Interfaces 7 (2015) 980–988.

[50] L.-L. Feng, M. Fan, Y. Wu, Y. Liu, G.-D. Li, H. Chen, W. Chen, D. Wang, X. Zou, J. Mater. Chem. A 4 (2016) 6860–6867.

[51] X. Tao, J. Wang, C. Liu, H. Wang, H. Yao, G. Zheng, Z.W. Seh, Q. Cai, W. Li, G. Zhou, Nat. Commun. 7 (2016) 11203.

[52] G. Zhou, H. Tian, Y. Jin, X. Tao, B. Liu, R. Zhang, Z.W. Seh, D. Zhuo, Y. Liu, J. Sun, J. Zhao, C. Zu, D.S. Wu, Q. Zhang, Y. Cui, Proc. Natl. Acad. Sci. USA 114 (2017) 840–845.

[53] X. Tang, Z. Sun, H. Yang, H. Fang, F. Wei, H.-M. Cheng, S. Zhuo, F. Li, J. Energy Chem. 31 (2019) 119–124.

[54] S.S. Zhang, J. Power Sources 231 (2013) 153–162.